DEPARTMENT OF PHYSICS, UNIVERSITY OF JYVÄSKYLÄ
RESEARCH REPORT No. 2/1993

RADIATION-INDUCED MAGNETIC FLUX LOSS IN PERMANENT MAGNETS

BY
OLLI-PEKKA KÄHKÖNEN

Academic Dissertation
for the Degree of
Doctor of Philosophy

Jyväskylä, Finland
December 1993

URN:ISBN:978-951-39-9484-6
ISBN 978-951-39-9484-6 (PDF)
ISSN 0075-465X

Jyväskylän yliopisto, 2023

ISBN 951-34-0145-6
ISSN 0075-465X

DEPARTMENT OF PHYSICS, UNIVERSITY OF JYVÄSKYLÄ
RESEARCH REPORT No. 2/1993

RADIATION-INDUCED MAGNETIC FLUX LOSS IN PERMANENT MAGNETS

BY
OLLI-PEKKA KÄHKÖNEN

Academic Dissertation
for the Degree of
Doctor of Philosophy

To be presented, by permission of the
Faculty of Mathematics and Natural Sciences
of the University of Jyväskylä,
for public examination in Auditorium S-212 of the
University of Jyväskylä on December 3, 1993,
at 12 o'clock noon

Jyväskylä, Finland
December 1993

Jyväskylä, September 1993

Preface

The studies in this thesis have been carried out at the Department of Physics of the University of Jyväskylä during the years 1989–1993. I wish to express my gratitude to associate professor Matti Manninen who has been supervising me during my work. I am also very grateful to Dr. Mikko Talvitie, Mr. Erkki Kautto, Dr. Hannu Rajainmäki, Dr. Seppo Mäkinen and professor Veikko Lindroos for fruitful collaboration. I want to thank Dr. Jaana Kumpulainen, Dr. Pauli Heikkinen and Dr. Juha Ärje for constructive discussions.

The Department of Physics has provided me with extremely good working conditions. I would like to thank the whole staff of the Department of Physics for the supporting atmosphere, and especially the members of the Solid State Group for their interest in my research. I would also like to thank the whole staff of the Accelerator Laboratory for their fruitful co-operation during my irradiation experiments.

The research stipendium from the University of Jyväskylä is gratefully acknowledged.

Jyväskylä, September 1993

Olli-Pekka Kähkönen

Abstract

This thesis reviews six publications studying the effects of radiation in permanent magnets. The radiation-induced magnetic flux loss has been measured in various types of experiment. The basic magnetic properties such as remanence (B_r), coercive force (H_c) and maximum energy product ($(BH)_{max}$) of the unalloyed Nd-Fe-B magnets has been measured at elevated temperatures. The magnetic flux loss has been measured as a function of the irradiation dose at 15 K and at 300 K with unalloyed and Nb- and Dy- alloyed Nd-Fe-B permanent magnets. The dependence of the radiation-induced magnetic flux loss on the irradiation temperature has been measured with proton and α-particle irradiations. The proton irradiations have been made in the temperature range of 20–300 K with Nd-Fe-B samples magnetized in two different ways and with Sm-Co permanent magnet samples at higher temperatures. In the α-particle irradiations we have used only one type of Nd-Fe-B samples. The dependence of the flux loss on the internal magnetic field has been studied using samples magnetized in different ways as well as doing the irradiations in an external magnetic field. The dependence of flux loss on the particle energy has been measured with 14–20 MeV proton beam. The experimental results show that the radiation-induced flux loss is highly dependent on the irradiation temperature and on the magnetic field inside the sample. We have developed a simple theoretical model to describe the mechanisms of the radiation-induced flux loss. The model is based on the assumption that the incoming particle collides with an atom of the crystal and causes a thermal spike in the crystal which allows a nucleation of a new domain in the opposite direction. The good agreement between experimental and theoretical results support our suggestion of the mechanism of radiation-induced magnetic flux loss.

List of publications

This thesis is a review of the following publications:

I O.-P. Kähkönen, S. Mäkinen, M. Talvitie, H. Rajainmäki and M. Manninen, *Temperature dependence of irradiation-induced magnetic flux loss in $Nd_2Fe_{14}B$ permanent magnets*, Europhysics Letters, **12** (1990) 413.
https//doi.org/10.1209/0295-5075/12/5/006

II S. Mäkinen, O.-P. Kähkönen and M. Manninen, *Positron self-trapping in $Nd_2Fe_{14}B$ crystal*, Journal of Physics: Condensed Matter **3** (1991) 2507.
https//doi.org/10.1088/0953-8984/3/15/005

III M. Talvitie, O.-P. Kähkönen, S. Mäkinen, H. Rajainmaki, M. Manninen and V. Lindroos, *Magnetic flux loss in Nd-Fe-B magnets irradiated with 20 MeV protons*, Journal of Magnetism and Magnetic Materials, **102** (1991) 323.
https://doi.org/10.1016/0304-8853(91)90146-2

IV O.-P. Kähkönen, S. Mäkinen, M. Talvitie and M. Manninen, *Radiation damage in Nd-Fe-B magnets: Temperature and shape effects*, Journal of Physics: Condensed Matter, **4** (1992) 1007.
https//doi.org/10.1088/0953-8984/4/4/011

V O.-P. Kähkönen, E. Kautto, M. Talvitie and M. Manninen, *Effects of high temperature irradiation on SmCo-permanent magnets*, Journal of Applied Physics, **72** (1992) 2075.
https://doi.org/10.1063/1.351641

VI O.-P. Kähkönen, M. Talvitie, E. Kautto and M. Manninen, *Effects of proton and α irradiations on permanent magnets*, JYFL preprint 19/93, submitted to Physical Review B.
https//doi.org/10.1103/physrevb.49.6052

The author has written all the papers, except papers **II** and **III**. He has done all irradiations, magnetic measurements and calculations concerning the radiation-induced magnetic flux loss, except the magnetic measurements with the hysteresisgraph.

Table of contents

1. Introduction 1

2. Basic properties of the rare-earth magnets 4

2.1. General theory of rare-earth magnetism 4

2.2. Main phases of the Nd-Fe-B and Sm-Co permanent magnets 8

3. Experiments 11

3.1. Sample preparation 11

3.2. Magnetic measurements 12

3.3. Irradiation techniques 13

3.4. Irradiation experiments 14

3.5. Discussion 21

4. Theory 23

4.1. Irradiation-induced magnetic flux loss 23

4.2. Numerical calculations 27

5. Results 28

5.1. Hysteresis measurements 28

5.2. Results of the irradiation experiments and calculations 29

6. Discussion and concluding remarks 35

References 37

1. Introduction

Since 1984, when the high-performance permanent magnet material $Nd_2Fe_{14}B$ was discovered, basic research of the rare-earth magnetism has increased rapidly. Nowadays several other phases based on rare-earth transition-metal alloys, with an atomic structure similar to $Nd_2Fe_{14}B$, have been studied widely. The lattice structure, electronic and magnetic properties as well as the applications of these materials have aroused scientific interest around the world. This is basically due to the excellent magnetic properties of the $Nd_2Fe_{14}B$ phase when compared to any other commercially available permanent magnet materials. Another reason is probably the low cost of their raw materials [1].

One of the applications of permanent magnets is to use them in the particle accelerators. Permanent magnets can be used in the beam-focussing devices and in the beam wigglers in synchrotron technology. However, it has been found in earlier studies that the $Nd_2Fe_{14}B$ magnets are more sensitive to the particle radiation than the widely used SmCo permanent magnets [2-4]. The magnetization drops at the room temperature very quickly when the permanent magnet sample is placed in the particle beam. This is a drawback because it can prevent the usage of the $Nd_2Fe_{14}B$ permanent magnets radiative conditions. Another area of the applications where the particle radiation should be taken into account, is the space technology. Although several irradiation studies of the $Nd_2Fe_{14}B$ permanent magnets have been done, the mechanism which produces the radiation damages of the magnetization is not well understood. On the other hand, the sensitivity to the particle radiation opens up a new possibility for basic research to study the domain nucleation and the demagnetization processes in permanent magnets.

In this work we have concentrated on the experimental study of the basic properties and

mechanisms of the irradiation-induced demagnetization of $Nd_2Fe_{14}B$ permanent magnets. Some of the experiments have been done with the $SmCo_5$ permanent magnets to look for the differences between these two different types of magnet. Based on these experimental studies we have also introduced a theoretical model for the demagnetization mechanism of the particle irradiation.

The irradiations of this work have been carried out at the Department of Physics of the University of Jyväskylä. The main part of the irradiations has been done using the proton beam from the MC-20 cyclotron. The old MC-20 cyclotron was closed down during this study and therefore one experiment with an α-particle beam has been carried out with the new K-130 heavy ion cyclotron.

We have studied various properties of irradiation effects in permanent magnets. The dependence of the flux loss on the dose and on the irradiation temperature has been observed. The dependence of the flux loss on the internal magnetic field has been verified by studies where the shape of the sample has been changed or an external magnetic field has been used. The theoretical work is based on these studies and it can explain the experimental results at least qualitatively.

The most important result is the temperature dependence of the irradiation-induced flux loss, which has been measured in both types of the studied material. The $Nd_2Fe_{14}B$ magnets can withstand radiation at low temperatures with no remarkable flux loss. The flux loss is greater if the irradiations are made at higher temperatures. The same feature was found in $SmCo_5$ magnets but at temperatures above the room temperature. The flux loss increases if the irradiation temperature increases. In both types of magnet the mechanism of the flux loss seems to be the same. The mechanism is described by the theory as follows: the incoming particle heats the magnet sample locally and opens up a possibility of the domain nucleation in opposite direction. The nucleation of the new domain depends on the magnetic field inside the magnet sample. The internal magnetic field is dependent on the shape of the magnet. Thus the magnetic flux loss induced by

the irradiation is also dependent on the shape of the magnet sample. This dependence was also found in our experimental work.

Although our theoretical model is quite simple, it can explain the experimental results. The good agreement between the experimental results and the theoretical calculations supports our model for the origin of the magnetic flux loss caused by particle irradiation.

2. Basic properties of rare-earth magnets

There is a large number of theories describing the magnetism of rare-earth (R) atoms and rare-earth transition-metal (RT) alloys. We are not going to survey all of them in detail but give an overview of theories relevant to the present work. In section 2.2. the crystallographic structures and basic magnetic properties of $Nd_2Fe_{14}B$ and $SmCo_5$ phases are introduced.

2.1. General theory of rare-earth magnetism

The elements from lanthanum to lutetium (atomic numbers from $Z = 57$ to $Z = 71$) are called rare-earth metals. They are characterized by the filling up of the $4f$ electronic shell. Lanthanum has no $4f$ electrons and lutetium has 14 $4f$ electrons. The electron configuration in the free rare-earth atom is $(\mathrm{Pd})^{46}\ 4f^n\ 5s^2\ 5p^6\ 5d^1\ 6s^2$, where n is the number of $4f$ electrons. It is assumed that the magnetic moment of the rare-earth atoms comes directly from the $4f$ electrons and it is also assumed that the ground state of the $4f$ shell is determined by the Hund's rule. This means that the total angular momentum J of the $4f$ shell is $J = L-S$ for light rare-earth elements and $J = L+S$ for heavy rare-earth elements, where L and S correspond to the orbital angular momentum and spin, respectively [1,5]. The magnetic moment is defined as

$$\boldsymbol{\mu} = \mu_{\mathrm{B}}(\boldsymbol{L} + 2\boldsymbol{S}), \tag{1}$$

where μ_{B} is the Bohr magneton [5].

The $5d$ and $6s$ electrons are valence electrons. They are delocalized and form the conduction band in the metallic state of the rare-earth elements. The $4f$ shell is well shielded by the full $5s$ and $6p$ shells against the outside perturbations and it is also

localized at the atom. The overlap between $4f$ wavefunctions of the neighboring atoms is very small [5].

The rare-earth and iron magnetic moments are coupled ferromagnetically for the light rare-earths and antiferromagnetically for the heavy rare-earths. The total R moment and R spin moment are antiparallel for the light rare-earths and parellel for the heavy rare-earths. Thus, the rare-earth $4f$ and iron $3d$ spin moments are always antiparallel, *i.e.* the $3d$–$4f$ exchange interaction is invariably antiferromagnetic [1].

One possibility to describe the $4f$–$3d$ coupling is to use the Ruderman-Kittel-Kasuya-Yosida type interactions [1] which are based on the polarization of the rare-earth s-band conduction electrons by the $4f$ electrons. However, this interaction mechanism is not able to describe the experimental results. Therefore interaction mechanisms where the $5d$ conduction electrons are taken into account were introduced. In these coupling models the positive local $5d$ momentum is assumed to be induced by the $4f$ spin. The final $4f$–$3d$ coupling is formed by the indirect $5d$–$3d$ exchange interactions [1].

To describe the more macroscopic properties of the rare-earth transition-metal alloys, such as magnetization processes and anisotropy, several models and theories have been devised. For example, the anisotropy in a ferromagnetic compound is described by the crystalline electric field (CEF) in combination with the rare-earth transition-metal exchange interactions. The Hamiltonian for the rare earth atom in an applied magnetic field H is

$$H_{\mathrm{R}}(i) = H_{\mathrm{CEF}}(i) + 2(g-1)\boldsymbol{J}\cdot\boldsymbol{H}_{\mathrm{ex}} + g\boldsymbol{J}\cdot\boldsymbol{H}, \tag{2}$$

where $H_{\mathrm{CEF}}(i)$ is the crystalline field Hamiltonian for each rare-earth atom, $\boldsymbol{H}_{\mathrm{ex}}$ is the effective exchange interaction field and g is the Landé factor [1,6].

However, when the properties of the real permanent magnets are discussed, also the microstructure of the material should be taken into account. The grain size of the main phase depends drastically on manufacturing methods. On the other hand, the grain

size influences the interactions between the grains and therefore also the properties of the magnetization processes [1].

Some words about the macroscopic magnetic properties of permanent magnets should be mentioned. In figure 1. the hysteresis loop of a permanent magnet is shown.

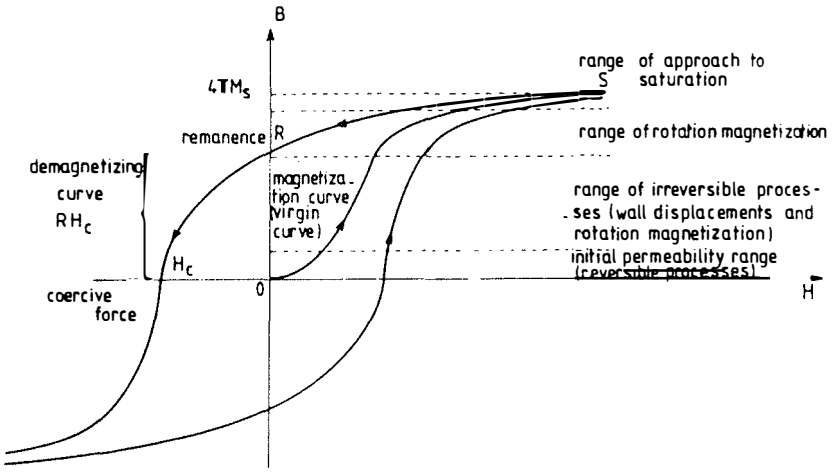

Figure 1. *The hysteresis loop of a permanent magnet* [7].

The remanence, B_r, is the value of magnetic induction (magnetization) which persists after the strength of the applied field H is reduced to zero from the value where the saturation of the magnetization is reached. The strength of the negative applied field reducing the remanence zero is defined as coercive field H_c. Permeability μ is defined as the ratio of the induced field B to the magnetizing field H [7].

During this work the concept of self-demagnetization has become important. When a permanent magnet is magnetized and removed from its magnetizing yoke, free poles are established. Between these two poles there exists now a field potential $-H_d$. The demagnetizing field is a result of the magnetic field lines, generated by the sample itself, penetrating the magnet antiparallel to the intrinsic magnetization B_i, thus reducing the total magnetic field inside the sample. When an external magnetic field H is applied

to the magnet the combined influence of the applied field and the internal field has to be considered [8-10]. The magnetic field required for the nucleation of a reversed domain in a magnet placed in an open air, H_n is the sum of the anisotropy field H_a and demagnetizing field H_d,

$$H_n = H_a + H_d. \tag{3}$$

The anisotropy field H_a is required for the magnetization reversal when only coherent rotation is allowed. H_d is proportional to the magnetization

$$H_d = \frac{(N_g + N_s)B_i}{\mu_0}, \tag{4}$$

where N_g is the demagnetization factor which is related to the microstructure, and N_s is the demagnetization factor which is dependent on the shape of the specimen. Replacing B_i/μ_0 with $4\pi M_s$, where M_s is the saturation magnetization, and taking into account that N_g is related to an individual grain which is saturated and that N_s is related to the magnetization of the whole magnet specimen, equation (4) can be written in the form

$$H_d = -N_g 4\pi M_s - N_s 4\pi M_{inst}, \tag{5}$$

where M_{inst} is the instantaneous value of the total magnetization of the magnet sample.

One way to estimate the value of the shape-dependent demagnetization factor N_s is to find out the load-line slope from the demagnetization curve. The load line-slope is defined as

$$\frac{B_d}{\mu_0 H_d} = 1 - \frac{1}{N_s}, \tag{6}$$

which is usually referred to as the unit permeance or the coefficient of self-demagnetization. The relationship between the demagnetization curve and the load-line slope is showed in figure 2.

For materials with a high coercive force the magnetization is approximately uniform from point to point. For simple geometries, such as uniformly magnetized cylinders, the demagnetization factors N have been derived [10].

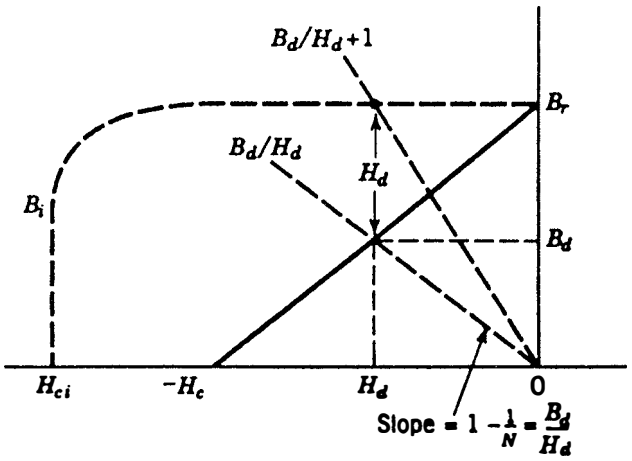

Figure 2. *The load line and the demagnetization curve of a magnet with high coercive force* [10].

2.2. Main phases of the Nd-Fe-B and Sm-Co permanent magnets

$Nd_2Fe_{14}B$ magnets

The main phase of the sintered Nd-Fe-B material is the $Nd_2Fe_{14}B$ phase. It has a complex crystallographic structure with 68 atoms in the unit cell. Fig. 3. shows the unit cell of $Nd_2Fe_{14}B$. Only four of the 56 iron atoms are on the planes $z = 0$ and $z =$ 0.5 c, where also the neodymium and boron atoms are lying. All the other iron atoms form puckered, hexagonal nets which lie between the z =0 and z = 0.5 c planes. The space group of $Nd_2Fe_{14}B$ is $P4_2/mnm$ [11].

As can be seen from Fig. 3. there are six Fe sites in the unit cell. These six Fe sublattices are assumed to be ferromagnetically coupled and they also form the main part of the magnetization of the whole crystal [1,12]. The main role of the Nd ions is

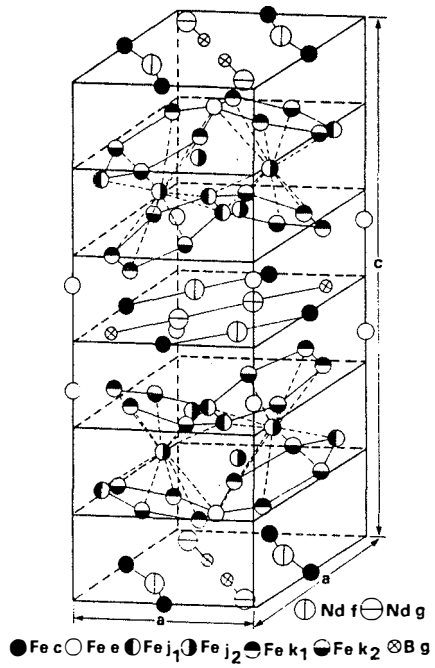

Figure 3. *The unit cell of the* $Nd_2Fe_{14}B$ *phase* [11].

connected to the anisotropy. The anisotropy energy is the energy needed to change the direction of the magnetization from the easy-axes (c-axes in the $Nd_2Fe_{14}B$ phase) to the hard direction. The four Nd ions are in two different sites in the unit cell. Because of the orthorhombic point symmetry of the crystalline electric field, all the four Nd ions have to be taken into account when constructing the crystal-field Hamiltonian for the Nd ions [1].

In sintered, fully magnetized samples the size of the magnetic domains is the same as the size of the grain. However, the domain walls between the different domains in a partially magnetized magnet can move very easily [1].

$SmCo_5$ magnets

As the $Nd_2Fe_{14}B$ magnets, sintered SmCo magnets have also a very complex crystallographic structure. The main phase in SmCo magnets is the hexagonal $CaCu_5$-type $SmCo_5$ phase with a space group $P6/mmm$. The unit cell of the $SmCo_5$ phase is shown

in figure 4.

The basic magnetic properties of $SmCo_5$ are similar to the ones of the $Nd_2Fe_{14}B$ magnets [5]. Concerning the irradiation effects there is one difference between these two types of magnet. The $SmCo_5$ phase does not have a light element which can absorb a larger energy in a collision than the heavier elements.

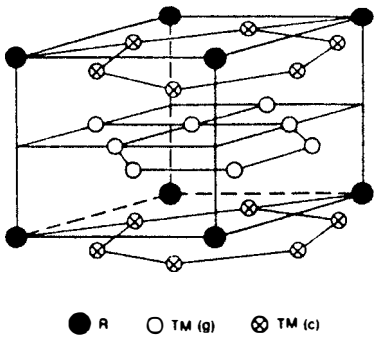

Figure 4. *The unit cell of the* $SmCo_5$ *phase* [1].

3. Experiments

3.1. Sample preparation

In this work we have used two different kinds of permanent magnet which are based on the Nd-Fe-B and Sm-Co alloys. Both types are made by the sintering method but only Nd-Fe-B magnets are manufactured by the cooperators of this work. The Sm-Co magnet samples were cut from commercial magnets.

In the sintering method the cast Nd-Fe-B alloys were crushed and milled to the average particle size of 3 μm. The powder was then axially compacted in a transverse magnetic field. This is to guarantee the right orientation of the grains in the magnet samples. The compacts were sintered at 1340 K in a vacuum furnace. The final step of the process was a heat treatment at 870 K. Part of the samples were high coercivity Dy- and Nb-alloyed magnets where part of the Nd atoms were substituted with Dy and part of the Fe atoms with Nb atoms. The mean grain size of the samples was about 10–30 μm depending on the alloying [13].

For the irradiations the samples were cut from a magnet block with a diamond saw to the size needed in the experiment. In most cases the sample size was about 7mm $\times$ 7mm $\times$ 1mm. The smallest samples used in the experiments were 1mm $\times$ 1mm $\times$ 1mm.

After the samples were cut to the right dimensions they were magnetized and measured with hysteresisgraph to check that the samples were fully magnetized.

In all the irradiation experiments the penetration depth of the projectile particle was approximately calculated by using the average penetration depth in pure elements and

the nominal composition of the alloy [14]. The sample thickness and the energy of the irradiation particle were chosen such that the particle would penetrate through the sample losing almost all of its energy in the sample but would not gather in the sample. In the case of the proton irradiation, the proton (H^+) gathering to the sample could have caused the formation of hybrids in the sample.

3.2. Magnetic measurements

To measure magnetic changes caused by the irradiations in the sample we have used two types of measurement techniques: The closed-circuit hysteresisgraph and the open-circuit induction method.

The hysteresisgraph was used to determine the remanence of the magnet sample after the samples were magnetized with a pulse-magnetizer having a magnetic field of about 10 T. The hysteresis graphs were measured before irradiations at the temperatures between 295 and 454 K with the KJSA TPF-1 high-temperature facility.

The hysteresisgraph has also been used to study if there persists irreversible microstructural changes by measuring the graph also after the irradiations.

The total magnetic flux of the samples was measured with the open-circuit method. The sample was passed through the induction coil and the induced voltage was measured over a resistor with a memory oscilloscope as a function of time. By integrating the voltage over the time, a value proportional to the magnetization in the sample was obtained. By measuring this value before and after the irradiation, the relative magnetic flux loss in the sample can be calculated.

3.3. Irradiation techniques

The main part of the irradiations were made with the MC-20 cyclotron of the University of Jyväskylä. The last irradiation experiment with α-particles was carried out with the new K-130 heavy-ion cyclotron.

In the irradiations we used three types of sample holder. In the first measurements, where the dose dependence of the flux loss was measured, the room-temperature sample holder and the cold-head sample holder were used. In the room-temperature sample holder the whole sample was irradiated with the ion beam. The ion current was measured directly from the sample holder. The sample was placed into the water-cooled holder and the ion current was kept below 20 nA. Thus no significant rise of the sample temperature was expected.

For the low-temperature measurements we have used a two-stage closed-cycle helium refrigerator. The temperature of this cooled sample holder is measured by an E-type thermocouple and controlled by a microcomputer. The temperature can be varied from 15 K to 300 K. In this case the ion current was measured with a Faraday cup between the sample holder and the beam collimator. Thus we were not able to measure the ion current while the ion beam was irradiating the sample. The irradiated area of the sample was 6 mm in diameter and therefore the samples were irradiated only in the central region. The ion current was measured after every 30 seconds to check the stability of the beam. However, the use of the Faraday cup gives us a better estimate of the irradiation dose than the direct ion-current measurement from the sample. The low-temperature facility was also used in the positron-lifetime experiments.

In the high-temperature experiments, designed to measure the temperature dependence of the flux loss in $SmCo_5$, we used a sample holder which was heated with a tungsten filament embedded in boron nitride. The temperature of the sample holder was mea-

sured with a C-type thermocouple and controlled with the Eurotherm PID-controller. The temperatures used varied from 300 K to 823 K. In this holder the ion current was measured directly from the the sample, but the sample was placed so that it would act like a Faraday cup. The irradiated area was 6 mm in diameter.

3.4. Irradiation experiments

Irradiation dose

The first experiment of this work was designed to study the dependence of the total magnetic flux in the permanent magnets on the irradiation dose [13,15]. In this experiment the total magnetic flux loss, induced by the proton irradiation, was measured from the unalloyed and dysprosium- and niobium-alloyed samples at room temperature and at 15 K. The size of the samples was 7.1 mm ×7.1 mm × 1.0 mm. The sample platelets were magnetized parallel to the shortest dimension. The energy of the projectile protons was 20 MeV which is enough for penetration through the sample without any proton (hydrogen) implantation into the sample.

In the case of the room-temperature measurements the ion current was measured directly from the sample but in the low-temperature measurements the ion current was measured with a movable Faraday cup. The use of the Faraday cup gives us a better estimate of the dose due to the secondary-electron emission or due to the other radiation effects which can perturb the measurement when the ion current is measured directly from the sample.

The results indicate that the $Nd_2Fe_{14}B$ magnets are extremely sensitive to proton irradiation at room temperature but can withstand proton irradiation much better at low temperatures. At the room temperature (300 K) the samples lost almost all of their magnetization with the doses over 10 Mrad. At the low temperature (15 K) the flux loss was only 17 % with a dose which is 1000 times larger than the dose needed for the

same flux loss at room temperature. To check that the different irradiation geometry of the low-temperature irradiations did not cause the differences in the results, we irradiated three samples at room temperature with the low-temperature sample holder. Only little difference between the two results of the room-temperature irradiations was observed. The reason for this difference was probably the difference in the ion-current measurements.

The samples made of the Dy- and Nb-alloyed material proved to be slightly better in withstanding proton irradiation, which might be due to their higher coercive force when compared to unalloyed samples.

Although the samples lost almost all of their magnetization when irradiated at room temperature with a dose over 10 Mrad, they could be remagnetized to their original state. The hysteresis loops were measured before and after the irradiations, and no significant changes were observed. This indicates that no permanent crystallographic damage appeared during the irradiation. The main result of these first experiments was the strong dependence of the magnetic flux loss on the irradiation temperature.

Irradiation temperature and magnetic orientation

In order to study in more detail the temperature dependence, we performed an experiment where the irradiation temperature was varied between temperatures used in the first experiment [16].

The irradiation setup was almost the same as used in the low-temperature irradiations earlier. The only difference was that the irradiation temperature was controlled by a microcomputer so that it was possible to keep the sample at fixed temperature between 15 K and 300 K.

In this irradiation experiment we used two kinds of Nd-Fe-B sample with different magnetic orientation. The size of both types of sample was 7.1 mm×7.1mm× 1.0mm. One

group of the samples was magnetized parallel to the direction of the shortest dimension of the sample, and the other group of samples was magnetized perpendicular to the shortest dimension. The permeance-coefficient, $(B/\mu_0 H)$, which depends on the shape and direction of the magnetization of the samples, was about -0.35 when magnetization was *parallel* to the shortest dimension and about -10 when the magnetization was *perpendicular* to the shortest dimension.

The direction of the proton beam was always parallel to the shortest dimension of the plate-shaped samples. Thus in the first group of the samples the direction of the magnetization was parallel to the direction of the proton beam, and in the other group of samples the beam was perpendicular to the magnetization. Using these two types of magnetization geometry we could get some information about the dependence of the irradiation-induced flux loss on the internal magnetic field of the sample. The dose of the proton irradiation was about $6.5 \cdot 10^{13}$ particles (100 Mrad). The dose was estimated from the results of the dose-dependence measurements, and it should cause about 50 % magnetic flux loss at room temperature when irradiated in the cold-head geometry.

The results of the irradiations with the samples magnetized parallel to the shortest dimension, show strong dependence on the irradiation temperature. The magnetic flux loss of the sample increased from a value less than 3 % to the value of about 35 % when the irradiation temperature was increased from about 15 K to the room temperature (300 K). However, the samples which were magnetized perpendicular to the shortest dimension (perpendicular to the ion beam, B/μ_0 H=-10) did not show any decrease in the magnetization at the irradiation temperatures of 25–300 K. This result indicates that the internal magnetic field affects the process of creation of magnetic damages. The hysteresis measurements did not show any changes in the hysteresis curve after the proton irradiations which indicates that no stable crystallographic changes appeared during the irradiations. The lattice defects were studied further with the positron-lifetime technique.

The dependence of the magnetic flux loss in the $SmCo_5$ material on the irradiation temperature shows nearly the same behaviour as in the case of the Nd-Fe-B-magnets [17]. The Nd-Fe-B magnets are sensitive to the particle irradiation much further beyond the Curie temperature (T_c=583 K) than the $SmCo_5$ magnets (T_c=997 K). The magnetic flux loss after the irradiation (100 Mrad) was about 45 % at 823 K and less than 10 % when the irradiation temperature was below 550 K. The result shows that the role of the light boron atom in the radiation sensitivity of the $Nd_2Fe_{14}B$ crystal is negligible.

To look more carefully at the dependence of the flux loss on the shape of the magnet sample, we did some 20 MeV proton irradiations with the 1 mm^3 cubic $Nd_2Fe_{14}B$ samples [16]. The cubic samples were irradiated at room temperature with doses of 5–1000 Mrad. The direction of the proton beam was either parallel or perpendicular to the direction of the magnetization. The flux loss after the 1000 Mrad irradiation was about 70 % when the direction of the proton beam was *parallel* to the ion beam and about 30 % when the direction of the magnetization was *perpendicular* to the ion beam.

The external magnetic field

The dependence of the flux loss on the internal magnetic field was studied by changing the external magnetic field with a package of permanent magnets placed near the sample during the irradiation [18]. The package contained one or three doped Nd-Fe-B permanent magnets with the size of 7.1 mm × 7.1 mm × 1.0 mm separated from the sample by an 0.5 mm thick indium plate. The remanence of the external permanent magnets was about 1.2 T. The positive direction of the external magnetic field (direction of the magnetization of the external magnet package) was the direction the magnetization of the sample. The direction of the external magnetic field was reversed by reversing the direction of the external magnet package. The strength of the external magnetic field was estimated by calculations based on the Biot-Savart law [19]. The estimated average value of the external magnetic field in the irradiated area, at the

middle plane of the sample, was about ± 0.138 T, created by one external permanent magnet, and about ± 0.285 T, created by the package of three external permanent magnets.

In this experiment the size of the samples was 7.1 mm × 7.1 mm × 0.5 mm, and the dose of the proton irradiation was $1.63 \cdot 10^{13}$ particles. The irradiations were made at room temperature (about 300 K).

The results of the irradiations in the external magnetic field show almost linear dependence on the external magnetic field. The remanent magnetization after irradiation decreases about 30 percentage points when the external magnetic field is changed from a value of about 0.3 T in the direction of the magnetization of the sample to a value of 0.3 T in the opposite direction to the magnetization of the sample. This result indicates a strong dependence of the magnetic flux loss on the magnetic field inside the irradiated sample.

Proton energy

For measuring the energy dependence of the irradiation-induced magnetic flux loss we used proton energies of 14, 16, 18 and 20 MeV [18]. The 14 MeV proton energy is the lowest energy required for the protons to penetrate through the 0.5 mm thick sample. Also in this experiment the size of the samples was 7.1 mm × 7.1 mm × 0.5 mm and the dose of the proton irradiation was about $1.63 \cdot 10^{13}$ particles. The irradiations were made at room temperature (about 300 K).

The variation of the proton energy in the range from 14 MeV to 20 MeV does not affect strongly the irradiation-induced magnetic flux loss. The experimental values of the remanent magnetization after the irradiation do not show a clear increase when the energy of the incoming proton decreases.

α-particle irradiations

The irradiations with the 56 MeV α particles were carried out in the new accelerator laboratory of Jyväskylä. In the irradiations we used the same cold-head geometry as was used in the temperature-dependence measurements in the context of the proton irradiations [18]. The sample size and the preparation method was the same as for the proton irradiation in the external magnetic field. The irradiation temperature was varied from 22 K to 295 K and it was controlled by the PC-based control system. The dose of the α particles irradiated into each sample was $1.0{\cdot}10^{13}$. The ion current used in the irradiations was less than 25 nA.

The remanent magnetization after the irradiation with a constant dose is increasing about 10 percentage points almost linearly from the value of 50 % when the irradiation temperature is decreasing from 300 K to about 150 K. Below 150 K the remanent magnetization increases more rapidly with the decreasing irradiation temperature having a value of over 90 % at 22 K. Below 150 K the temperature dependence of the experimental results seems to be different from the one above 150 K. This is probably due to the spin reorientation which occurs in the $Nd_2Fe_{14}B$ phase at 135 K. The spin reorientation changes the internal magnetic field which may influence the production mechanism of magnetic damages.

Positron-lifetime measurements

Possible changes in the microstructure caused by the particle irradiation were studied using the positron-lifetime technique. This technique has been widely used in studying lattice defects such as single vacancies, vacancy–impurity pairs and vacancy clusters. The probability of creation of vacancy-type defects by particle irradiation is very high and therefore we have to study if changes in microstructure could cause the magnetic flux loss induced by the particle irradiation.

The positron-lifetime measurements were done by using the JYFL low-temperature

facility [20,21]. The irradiation and measurement temperature can be adjusted to any temperature in the range of 15–300 K by using the two-stage helium refrigerator and a microcomputer-controlled heating system. This same cold head has also been used in the other low-temperature irradiations discussed above. The ^{22}NaCl positron source is enveloped in a thin Havar foil and mounted in a sample-source-sample sandwich geometry in the cold head. The thickness of the sintered, demagnetized $Nd_2Fe_{14}B$ samples was 0.5 mm which is enough to absorb more than 99 % of the positrons emitted by the source [22]. The measured spectra were analysed by using the Fortran programs RESOLUTION and POSITRONFIT [23].

Before irradiation the positron-lifetime spectra were measured at 15 K and at 300 K. The total dose of the proton irradiation was about $1.3{\cdot}10^{13}$ particles (20 Mrad). After the irradiation the positron lifetime spectra were measured at 15 K after annealing the samples at temperatures between 50 and 300 K in 50 K steps with an annealing rate of 25 K/h.

Before and after the irradiation two lifetime components were found at room temperature ($\tau_1 = (156 \pm 6)$ ps, $I_1 = (86 \pm 15)\%$ and $\tau_2 = (230 \pm 30)$ ps ,$I_2 = (14 \pm 15)\%$) and only one lifetime at 15 K ($\tau = (163 \pm 2)$). No changes were found in lifetimes during the annealing process: only one lifetime (163 ps) was found at 15 K after all annealings.

After the annealings the lifetime spectra were measured at temperatures between 15 and 300 K. The longer lifetime component appeared at a temperature about 150 K and no other lifetime components could be detected even at higher temperatures. This result indicates that no detectable amount of lattice defects caused by the irradiation could be found in the samples with this technique.

A detailed analysis of the lifetime spectra indicates that above 175 K two kinds of positron trap are present but below 125 K only one kind of positron trap is seen. The rapid increase in the intensity of the second lifetime around 150 K can be explained

by the presence of shallow traps of positrons, which can prevent the diffusion of the positrons into the deep traps (vacancies at the grain boundaries or in the main phase). Theoretical calculations show that polaron-like self-trapping becomes possible in the case of a perfect $Nd_2Fe_{14}B$ phase due to the complex crystallographic structure. The positron forms a polaron-like state in low-ion-density regions of the unit cell. The trapping of the positron into the vacancies at the grain boundary is allowed only at higher temperatures due to the strong temperature dependence of the polaron state. This theoretical result is in good agreement with the experimental results.

3.5. Discussion

The irradiation experiments reveal phenomena which should be taken into account when discussing the origin of magnetic damages in irradiated magnets. Firstly, the irradiation damage depends strongly on the irradiation temperature. Secondly, the temperature dependence of the flux loss is different in proton and α-particle irradiated $Nd_2Fe_{14}B$ magnets. Thirdly, the flux loss depends on the internal magnetic field *e.g.*, on the shape of the magnet sample, and also on the external magnetic field.

The results of the positron-lifetime experiments give us strong evidence that the crystallographic changes are not the reason for the irradiation-induced flux loss. This suggestion is supported by the fact that the irradiated magnets can be remagnetized to their original magnetization by an external magnetic field.

The dependence of the flux loss on the irradiation temperature in the α-particle irradiated Nd-Fe-B samples is different from that in the proton-irradiated samples. In the α-particle irradiated samples the temperature dependence is much weaker than in the proton-irradiated samples at temperatures above 150 K. This could be explained by the different amount of energy transfer from the irradiated ion to the lattice of the sample. In the proton-irradiated SmCo samples and Nd-Fe-B samples the dependence on the irradiation temperature is almost the same. The energy-transfer capacity of an

α particle in a knock-on collision is much bigger than that of the light proton.

Below 150 K also the α-particle irradiated samples were weakly sensitive to the irradiation. This can be explained by the spin-reorientation which reduces the internal magnetic field. The dependence on the internal magnetic field was also found in the irradiation experiments made in the external magnetic field, or by changing the shape of the sample.

One possibility to study these effects together is to look what happens in the sample when the irradiated particle comes in. An incoming positively charged particle feels the electrons of the crystal and its energy decreases during the penetration until it collides with a primary knock-on atom (PKA). In the collision it transfers part of its kinetic energy to the PKA. The energy of the PKA is then transferred to the lattice in a cascade of collisions between the PKA and the neighbouring atoms and, eventually, by the diffusion of heat. The temperature of the lattice rises quickly to a very high value during the collision cascade. The heat then diffuses into the lattice outside the collision region. When the temperature of the lattice is above the Curie temperature the spins are free to rotate. The internal magnetic field can now align the spins parallel to its direction. If the region where the temperature exceeds the Curie temperature is large enough, the nucleation of a new domain is possible. The direction of the internal magnetic field may be opposite to the magnetization due to the demagnetization field created by the magnet itself, and therefore also the magnetization of the new domain may be antiparallel to the magnetization. In that case part of the magnetization is lost when the domain grows to the size of the grain. In permanent magnets the domain walls are almost free to move and the growth of a domain is highly possible. In this model the effect of the internal magnetic field is clear. In the next chapter we introduce a theoretical model based on these suggestions.

4. Theory

4.1. Irradiation-induced magnetic flux loss

As described in chapter 2., the permanent-magnet materials based, on the rare-earth transition-metal alloys, have a very complex crystallographic structure, especially the $Nd_2Fe_{14}B$ phase having 68 atoms in the unit cell. Also the magnetic interactions between the atoms in the lattice are difficult to handle due to the complex lattice structure and due to the many-body interactions of the electrons.

Because of the difficulties in handling a large number of particles with many-body interactions by, for example, molecular-dynamic simulations, we have decided to use a more macroscopic way to model the origination mechanism of the irradiation-induced magnetic damages. The basic assumption of the model is that part of the energy of the incoming particle is transferred to the primary knock-on atom by the Coulomb interaction. The energy of the PKA is then transferred to the lattice in a collision cascade. The temperature of the lattice rises quickly to a very high value in a spherical region near the collision centre. Heat then diffuses into the lattice raising the temperature of the lattice locally above the Curie temperature. While the temperature of the lattice is above the Curie temperature the spins are free to rotate. An internal magnetic field can now align the spins along its direction. If the region, where the temperature is above the Curie temperature, is large enough the nucleation of a new domain is possible. If the magnetization direction of the new domain is opposite to the magnetization of the sample, part of the total magnetization is lost.

The nucleation of a new domain is possible if the volume of the sphere where the temperature is above the Curie temperature (T_c) is larger than the critical size of a

nucleation centre, described here by a critical radius R. A method for estimation of the critical radius is described in detail later in this chapter.

The minimum collision energy required to heat the sphere of radius R to the critical temperature T_c is calculated as follows. We assume that the primary knock-on atom causes a thermal spike and use the differential equation of heat transfer to describe the energy diffusion in the lattice. The equation of heat transfer can be written as

$$\frac{\partial T}{\partial t} = a^2 \nabla^2 T, \tag{7}$$

where a is a constant describing the heat-transfer capability of the lattice. The temperature distribution in the lattice after the collision is assumed to be a δ function. By using the Green's function technique, eq. (1) can be immediately solved to give

$$T(r,t) = (T_1 - T_0)\left(\frac{d^2}{4\pi a^2 t}\right)^{\frac{3}{2}} e^{-r^2/4a^2 t} + T_0, \tag{8}$$

where T_1 is the initial temperature of the primary knock-on atom, d^3 is the volume of one atom, and T_0 is the initial temperature of the sample. By finding the maximum R which satisfies the equation $T(R,t) = T_c$, we obtain the maximum radius of the region which is heated above the Curie temperature T_c:

$$T_1 = T_0 + (T_c - T_0)\left(\frac{2\pi R^2}{3d^2 e^{-1}}\right)^{\frac{3}{2}}. \tag{9}$$

It should be noted that equation (9) is independent of the thermal conductivity of the lattice.

The relation of T_1 to the kinetic energy of the primary knock-on atom is

$$E_{\text{kin}} = \frac{3}{2} k_B (T_1 - T_0). \tag{10}$$

Now the minimum kinetic energy needed, for a sphere of radius R to be heated above the Curie temperature, is determined by equations (9) and (10).

To determine the probability of a collision which can transfer the minimum energy to the primary knock-on atom, we have to find out first the minimum scattering angle

from the equation of energy transfer of a two-body elastic collision,

$$E_{\mathrm{kin}} = E_{\mathrm{i}}(1 - \frac{(\cos\Theta + (\frac{m_2}{m_1} - \sin^2\Theta)^{\frac{1}{2}})^2}{(\frac{m_2}{m_1} + 1)^2}), \tag{11}$$

where E_{i} is the energy of the incoming particle, Θ the scattering angle, m_1 the mass of the incoming particle and m_2 the mass of the target atom. Eq. (11) determines the minimum angle, Θ_{min}, which gives energy transfer larger than E_{kin}.

The scattering of the ions is assumed to be Coulomb scattering. The cross section, σ, for events giving energy larger than a particular E_{kin} can now be obtained by integrating the Coulomb-scattering cross section over angles larger than Θ_{min}:

$$\sigma = 2\pi q^2(\frac{1}{1 - \cos\Theta_{\mathrm{min}}} - \frac{1}{2}), \tag{12}$$

where

$$q = \frac{zZe^2}{2 \cdot 4\pi\epsilon_0(\frac{1}{2}mv_0^2)}$$

The total cross section is $\Sigma = n\sigma$, where n is the ion density of the sample. The probability of one collision is

$$P = L\Sigma = n\sigma L, \tag{13}$$

where L is the sample thickness.

We assume that each such collision causes domain nucleation in opposite direction and that the domain immediately grows to the size of the grain. The relative loss of magnetization can thus be calculated as

$$\frac{\Delta M}{M} = 2\frac{V_{\mathrm{grain}}}{V_{\mathrm{sample}}}PN_{\mathrm{p}}, \tag{14}$$

where N_{p} is the number of incoming particles and V_{grain} and V_{sample} are the grain and sample volumes, respectively.

By exploiting the method used in determining the nucleation volume in magnetic viscosity measurements [1, 24], we can now determine the critical size of the nucleation centre. The intrinsic coercive field H_{ci} is estimated using the relation [1]

$$H_{\mathrm{ci}} = \frac{c\sigma_{\mathrm{w}}}{V_{\mathrm{a}}^{1/3}M_{\mathrm{s}}} - N(4\pi M_{\mathrm{s}}), \tag{15}$$

where σ_w is the domain-wall energy density, V_a the activation volume, M_s the saturation magnetization, N is an appropriate demagnetization factor and c is a free parameter. By using equation (15) we can derive the radius of the nucleation centre in the external magnetic field and in open air. Equation (15) can now be written, as in section 2.1., in the form

$$-H_{ext} = \frac{c\sigma_w}{(\frac{4}{3}\pi)^{1/3} R M_s} - N_g 4\pi M_s - N_s 4\pi M, \qquad (16)$$

where H_{ext} is the external magnetic field (positive direction is that of the magnetization in the sample), R the critical radius of the spherical nucleation centre, N_g the demagnetization factor representing demagnetization fields created by the microstructure, N_s the demagnetization factor connected with the macroscopic shape of the sample and M the total average magnetization of the sample which changes during the irradiation. The first term represents the local internal magnetic field required to nucleate a new domain in reverse direction within a spherical region of radius R. We assume that each grain contains one magnetic domain with saturated magnetization and therefore we have used the value of the saturation magnetization in the second term. The estimation of the activation volume does not take into account effects caused by the grain boundary. These effects may decrease the anisotropy field near the boundary and reduce the magnetic-field value required to nucleate a new domain. However, when we are dealing with radiation-induced nucleation we can not distinguish the boundary region from the bulk.

From eq. (16) we can easily derive the radius of the activation volume for the simulations. Substituting $4\pi M_s$=1.6 T for the saturation magnetization of the $Nd_2Fe_{14}B$ phase and $4\pi M$=1.2 T for the total magnetization of the sample (and converting the units with $[T^2] = 79.58 \cdot 10^4 [J/m^3]$) we can calculate the critical radius as

$$R = \frac{c\sigma_w 4\pi}{(\frac{4}{3}\pi)^{1/3} 1.6\ (-\frac{H_{ext}}{[T]} + N_g 1.6\ + N_s 1.2\ M_t) 79.58 \cdot 10^4 [J/m^3]}\ , \qquad (17)$$

where M_t represents the relative total magnetization of the sample during the irradiation.

In the computations the sample is discretized in thin slices for a better estimation of the energy loss of the incoming particle during the penetration. The dose of the irradiation is divided into several parts, and the total magnetization of the sample is calculated after each of these parts taking into account the change in the critical size of the nucleation centre due to the changes in the total magnetization. The calculation method is described in detail in the next section.

4.2. Numerical calculations

For the numerical calculation of irradiation-induced magnetic flux loss we have developed a Fortran program. The energy distribution of the incoming particle is first determined. The sample is discretized in thin slices and the energy loss in each slice is calculated using the decreased final energy after each slice as initial energy for the next slice. The subroutine which calculates the energy loss in each slice is based on the tables of stopping and ranges of ions in matter [14]. We assume that only one type of PKA is important in the collisions. For example in the calculations of the Nd-Fe-B magnets we use only Fe atoms as PKA. (The calculations with boron as the PKA give us reasonable results in the case of Nd-Fe-B; however, the experiments with Sm-Co show that the light atoms are not important in the collisions.)

Before the calculation of magnetic flux loss the initial value of the critical size of the nucleation centre is calculated using eq. (17). The dose of the incoming particles is discretized in several parts and the decrease of the total magnetization is calculated after each of these parts in the way described above. Also the new value for the critical size of the nucleation centre is calculated after each part of the dose.

5. Results

5.1. Hysteresis measurements

The results of the hysteresis measurements at elevated temperatures are shown in figure 5. The intrinsic coercive force decreases over 50 % of its room-temperature value when the temperature is increased to 350 K. At 450 K the value of the intrinsic coercive force is less than 10 % of its initial value. The hysteresis curves measured after the proton irradiation did not show any changes. This result indicates that the dose used did not cause any permanent microstructural changes which could influence the hysteresis curves.

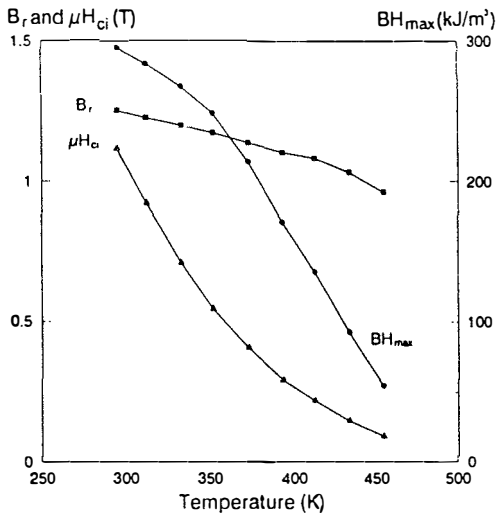

Figure 5. *The remanence (B_r), intrinsic coercive force ($\mu_0 H_{ci}$) and maximum energy product ($(BH)_{max}$) of* $Nd_2Fe_{14}B$ *magnets at elevated temperatures* [13].

The results reported for fast neutrons [4] show that the intrinsic coercive force is increasing during the neutron irradiation. This effect was suggested to originate from the

formation of defects which could reduce the mobility of domain walls or prevent the nucleation of new domains. We did not find this effect in proton-irradiated samples.

5.2. Results of the irradiation experiments and calculations

The dependence on the irradiation temperature was found in both α-particle- and proton-irradiated Nd-Fe-B samples at temperatures below 300 K. In figures 6 and 7 are shown the experimental results of the magnetic flux loss as a function of the irradiation temperature for proton and α-particle irradiation, respectively. The results of proton irradiations with the constant particle dose of $6.5 \cdot 10^{13}$ in the temperature range 15–300 K indicate that the flux loss decreases from the value of about 35 % to a value less than 5 % when the irradiation temperature decreases from 300 K to 15 K. The value of the unit permeance of these samples was $B/\mu_0 H$=-0.35. In the case of the samples with $B/\mu_0 H$=-10 no changes were found in the magnetization after the irradiation.

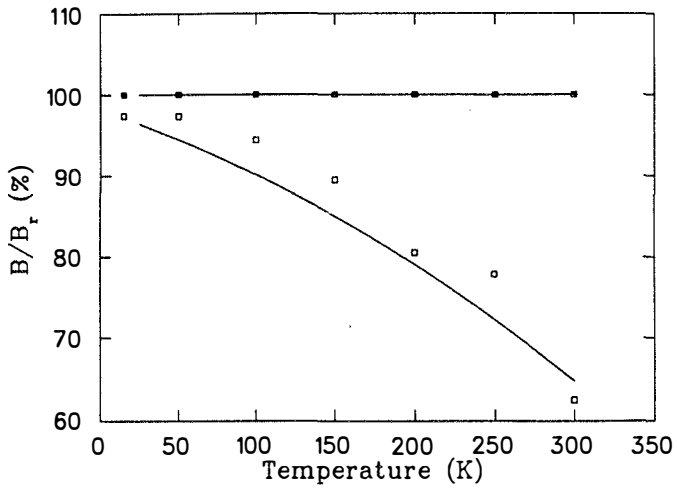

Figure 6. *The remanent magnetization of the* $Nd_2Fe_{14}B$ *magnet samples after the proton irradiation as a function of the irradiation temperature. The dots and the solid line represent the results of experiments and calculations, respectively* [18].

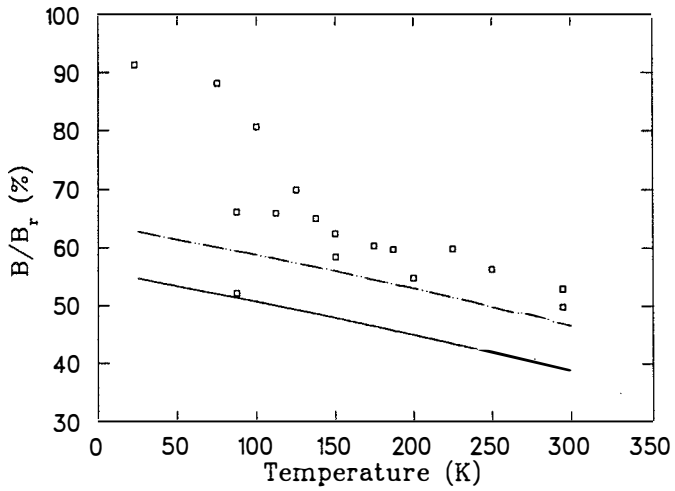

Figure 7. *The remanent magnetization of the* $Nd_2Fe_{14}B$ *magnet samples after the* α*-particle irradiation as a function of the irradiation temperature. The dots represent the results of experiments and the solid line and dashed line represent the results of calculations* [18].

After α-particle irradiation with a constant dose ($1.0 \cdot 10^{13}$) the flux loss decreases slowly: from the value of about 50 % to 40 % when the irradiation temperature decreases from 300 K to 150 K. Below 150 K the flux loss decreases more rapidly having a value of about 10 % at 22 K. The difference between the results of the proton and α-particle irradiations above 150 K is probably due to the fact that α particles are capable of transfering more energy to the PKA than the light protons.

The calculated results of irradiation-induced flux loss as a function of the irradiation temperature are also shown in figures 6 and 7. The values of the parameters used in the simulations for the $Nd_2Fe_{14}B$ magnets were D_g=3.5 μm, N_g=1 and c=0.35. The parameter N_g is dependent on the microstructure of the magnetic alloy and its value is N_g=2 for the $SmCo_5$ magnets [26].

The parameter N_s is dependent on the shape of the sample and we have used shape-dependent values of N_s as follows: N_s=0.74 for the samples with $B/\mu_0 H$=-0.35, N_s=0.09 for the samples with $B/\mu_0 H$=-10, both irradiated with protons, and N_s=0.9 for the samples with $B/\mu_0 H$=-0.18, irradiated with α particles. For the domain-wall energy density of the $Nd_2Fe_{14}B$ phase we used $\sigma_w=30\cdot10^{-3}$ J/m^2 [1].

The calculated results of the proton-irradiation-induced magnetic flux loss in the Nd-Fe-B magnets are in good agreement with the experimental results. For the samples with N_s=0.74 the calculated flux loss fits well the experimental results. Calculation with N_s=0.09 did not show any decrease in the magnetization, in agreement with the experimental data.

For the α-particle irradiations above 150 K the slope of the calculated magnetization curve is clearly almost the same as that of the experimental points. However, there is a difference in the absolute values of the magnetization between the calculations and the experiments above 150 K. This difference might be due to systematic errors in experimental estimation of the irradiation dose. Decreasing the value of the parameter D_g from 3.5 μm to 3.0 μm the difference between calculations and experiments vanishes (the dashed line in Fig. 7.), which indicates differences in microstructure between the α-particle irradiated samples and the proton-irradiated samples.

Below 150 K the temperature dependence of the experimental results seems to differ from the calculated predictions. This is probably due to the spin reorientation which occurs in the $Nd_2Fe_{14}B$ phase at 135 K. The spin reorientation changes the internal magnetic field which affects the process of domain nucleation. These effects are not included in our theoretical model.

In figure 8 are shown the experimental and theoretical results of the proton irradiations of the $SmCo_5$ magnets at elevated temperatures. At room temperature (307 K) only a slight decrease of magnetization was obtained as a result of the irradiation dose of about

$6.5 \cdot 10^{13}$ protons (98 Mrad, E=19.5 MeV). However, when the irradiation temperature was increased the flux loss increased. At the temperature of 823 K the remanent magnetization reduced to about 56 % due to thermal effects alone and to about 30 % due to both irradiation and thermal effects. The irradiation-induced magnetic flux loss has been separated from the thermal effects by assuming that the thermal effects decrease the magnetization before the irradiation, and the total magnetic flux loss, induced by irradiations, is measured starting from this lowered level of magnetization. As a result the remanent magnetization was about 53 % after the irradiation at 823 K.

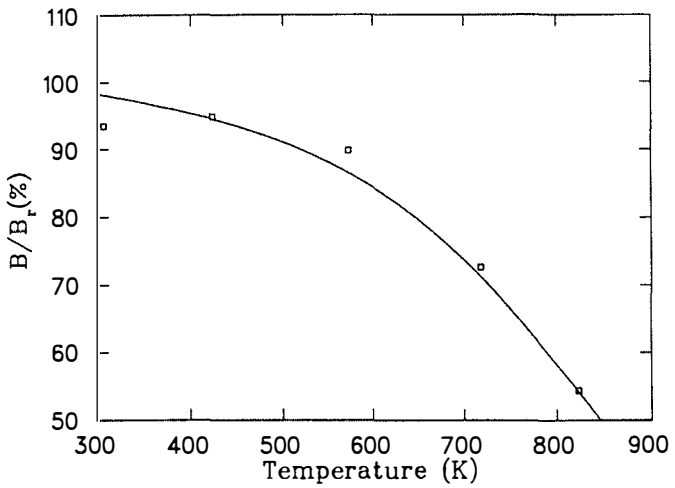

Figure 8. *The remanent magnetization of the* $SmCo_5$ *magnet samples after the proton irradiation as a function of the irradiation temperature. The dots and the solid line represent the results of experiments and calculations, respectively* [18].

In the calculations of the SmCo magnets we used the value σ_w=74·10^{-3} J/ m^2 for the energy density of the domain wall [25]. The other parameters giving the best fit to the experimental results, were D_g=1.6 μm, N_s=0.75, N_g=2, c=0.07, $4\pi M_s$=0.88 T and $4\pi M$=0.88 T.

The strong dependence of flux loss on the irradiation temperature for $SmCo_5$ supports

the conclusion that the light boron in the $Nd_2Fe_{14}B$ phase does not greatly influence the generation mechanism of radiation damages. The atomic weights of Sm and Co correspond to the atomic weights of Nd and Fe, respectively, but the $SmCo_5$ phase does not have any light elements.

The dependence of irradiation-induced magnetic flux loss on the internal magnetic field was studied in the temperature-dependence experiments where we used two samples with different magnetic orientation. To look more carefully into the effects of the changes in the internal magnetic field, irradiations in an external magnetic field were carried out. In figure 9 is shown the remanent magnetization of a sample after irradiation as a function of the strength of the external magnetic field. The calculations (solid line), with values of parameters taken from the α-particle-irradiation calculations, fit well to the experimental results. The remanent magnetization decreases almost linearly when the external magnetic field is increasing antiparallel to the magnetization of the sample and increases when the external magnetic field is oriented parallel to the magnetization of the sample.

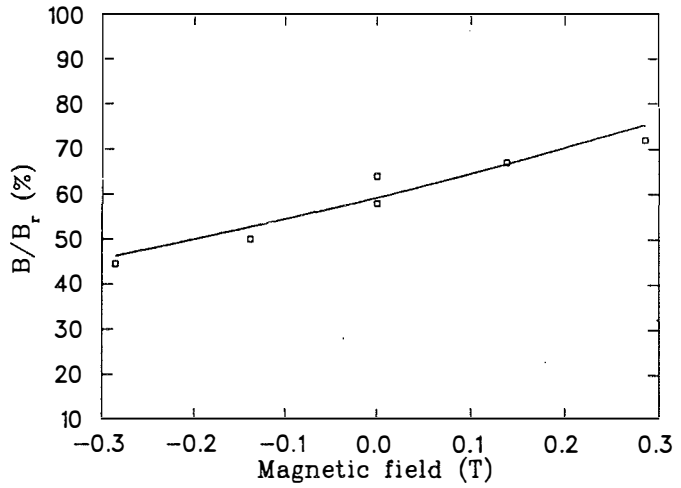

Figure 9. *The remanent magnetization of the* $Nd_2Fe_{14}B$ *magnet samples after the proton irradiation as a function of the strength of the external magnetic field. The dots and the solid line represent the results of experiments and calculations, respectively* [18].

Based on the calculations we assume that the strong dependence on the internal magnetic field is connected with the critical size of a nucleation centre. In eq. (17) the external magnetic field affects directly the size of the nucleation centre by decreasing the radius when the external magnetic field is increased in the opposite direction to the magnetization.

The dependence on the particle energy seems not to be very strong. In figure 10 is shown the remanent magnetization as a function of the proton energy. In the experimental results no remarkable changes were found in the energy region of 14–20 MeV. Although the calculated remanent magnetization after the proton irradiation shows a clear increase when the energy of the incoming proton decreases, the difference between the experiments and calculations is not so large for proton energies above 16 MeV.

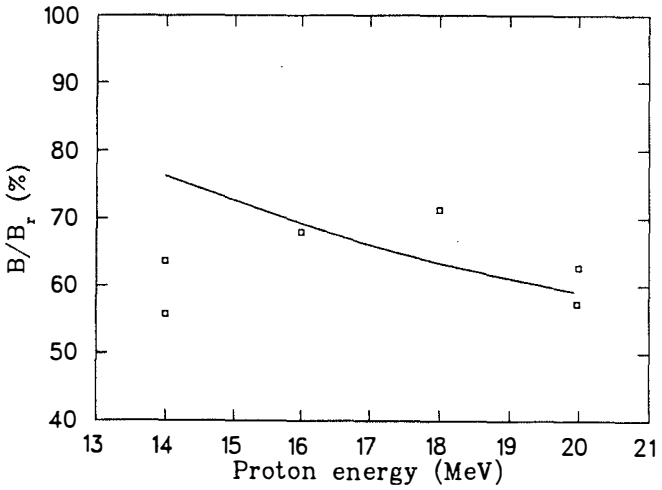

Figure 10. *The remanent magnetization of the* $Nd_2Fe_{14}B$ *magnet samples after the proton irradiation as a function of the proton energy. The dots and the solid line represent the results of experiments and calculations, respectively* [18].

6. Discussion and concluding remarks

The main role in the origin of the irradiation-induced magnetic damages seems to be played by the internal magnetic field. The effect of the internal magnetic field was detected in experiments where the irradiations were made in an external magnetic field, as well as in the temperature-dependence experiment where two types of sample with different magnetic orientation were used. Also the anomaly in the results of the temperature-dependence experiment with α particles at about 150 K, which is suggested to occur due to the spin reorientation of the $Nd_2Fe_{14}B$ phase, is an indication that the magnetic field inside an irradiated sample affects the demagnetization process.

In the introduced theoretical model the role of the internal magnetic field is evident from eqs. (16) and (17). The critical radius of the nucleation centre is dependent on the external magnetic field and on the demagnetization field created by the magnet specimen itself. The self-demagnetization is a result of the free poles established when the magnetic specimen is in the open air, and it is dependent on the magnetization and also on the macroscopic shape of the specimen. It should be noted that the dependence of the self-demagnetization on the magnetization affects the critical size of the nucleation centre: the radius increases when magnetization is decreasing due to the irradiation.

The internal magnetic field has an effect only in the hot region induced by a collision between the incoming particle and an atom of the crystal. It is assumed that the time, during which the lattice is above the Curie temperature, is long enough for the spins to rotate and reorientate along the internal magnetic field.

In the theoretical model the dependence on the irradiation temperature comes directly from the difference between the Curie temperature and the irradiation temperature. The difference increases when the irradiation temperature decreases requiring more en-

ergy to be transferred to the lattice. Thus, the probability of collisions with enough transferred energy is smaller at lower temperatures. However, when the proton- and α-particle-irradiation results of the temperature-dependence experiments are compared, a clear difference between the slopes can be seen. The remanent magnetization increases with decreasing temperature more rapidly after the proton irradiation than after the α-particle irradiation. A possible explanation to this phenomenon is the stronger capability of the heavier α particle to transfer energy when compared the light proton.

The results for the proton-irradiated $SmCo_5$ magnets show similar dependence on the irradiation temperature than that found in proton-irradiated $Nd_2Fe_{14}B$ magnets. This result indicates that the light boron atoms in the $Nd_2Fe_{14}B$ phase do not play any important role in the demagnetization process. The calculations show that only one type of atoms, Fe in the $Nd_2Fe_{14}B$ phase and Co in the $SmCo_5$ phase is needed as a primary knock on atom. The reason for this is that the energy transfer to the much heavier rare-earth atoms is smaller than to the Fe or Co atoms and, in addition the amount of rare-earth atoms in a lattice is smaller than the amount of transition-metal atoms.

References

[1] J. F. Herbst, Rev. Mod. Phys. **63**, (1991) 819.

[2] E. W. Blackmore, IEEE Trans. Nucl. Sci, **NS-32** (1985) 3669.

[3] A. F. Zeller and J. A. Nolen, Annual Report 1986, National Superconducting Cyclotron Laboratory, Michigan State University, USA, p. 161.

[4] J. R. Cost, R. D. Brown, A. L. Giorgi and J. T. Stanley, IEEE Trans. Magn., **MAG-24** (1988) 2016.

[5] J. Pierre, *Magnetism of Metals and Alloys*, ed. M. Cyrot, (North-Holland Publishing Company, 1982) p. 245.

[6] M. Yamada, H. Kato, H. Yamamoto and Y. Nakagawa, Phys. Rev. B, **38** (1988) 620.

[7] M. Kleman, *Magnetism of Metals and Alloys*, ed. M. Cyrot, (North-Holland Publishing Company, 1982) p. 535.

[8] R. Ramesh and K. Srikrishna, J. Appl. Phys., **64** (1988) 6406.

[9] M. Sagawa and S. Hirosawa, *High Performance Permanent Magnet Materials,* ed. S. G. Sankar, J. F. Herbst and N. C Koon, (Materials Research Society Symposia Proceedings, Vol.**96** Materials Research Society, Pittsburgh, Penn, 1987).

[10] R. J. Parker, Advances in Permanent Magnetism (Wiley, New York, 1990).

[11] J. F. Herbst, J. J. Croat, F. E. Pinkerton and W.B. Yelon, Phys. Rev. B, **29** (1984) 4176.

[12] Zong-Quan Gu and W. Y. Ching, Phys. Rev. B, **36** (1987) 8530,

[13] M. Talvitie, O.-P. Kähkönen, S. Mäkinen, H. Rajainmaki, M. Manninen and V. Lindroos, J. Magn. Magn. Mater., **102** (1991) 323.

[14] J. F. Ziegler, J. P. Biersack and U. Littmark, *The Stopping and Ranges of Ions in Matter*, (Pergamon Press, New York) 1985.

[15] O.-P. Kähkönen, S. Mäkinen, M. Talvitie, H. Rajainmäki and M. Manninen, Europhys. Lett., **12** (1990) 413.

[16] O.-P. Kähkönen, S. Mäkinen, M. Talvitie and M. Manninen, J. Phys. Condensed Matter, **4** (1992) 1007.

[17] O.-P. Kähkönen, E. Kautto, M. Talvitie and M. Manninen, J. Appl. Phys., **72** (1992) 2075.

[18] O.-P. Kähkönen, M. Talvitie, E. Kautto and M. Manninen, JYFL preprint 19/93, submitted to Phys. Rev. B.

[19] P. Heikkinen, private communication.

[20] S. Mäkinen, O.-P. Kähkönen and M. Manninen, J. Phys. Condensed Matter, **3** (1991) 2507.

[21] H. E. Hansen, R. Talja, H. Rajainmäki, H. K. Nielsen, B. Nielsen and R. M. Nieminen, Appl. Phys. A, **36** (1985) 81.

[22] S. Linderoth, H. E. Hansen, B. Nielsen and K. Petersen, Appl. Phys. A, **33** (1984) 25.

[23] P. Kirkegeerd, M. Eldrup, O. E. Mogensen and N. J. Pedersen, Comput. Phys. Commun., **23** (1981) 307.

[24] D. Givord, P. Tenaud and T. Viadieu, IEEE Trans. Magn., **MAG-24** (1988) 1921.

[25] A. Menth, H. Nagel and R. S. Perkins, Ann. Rev. Mater. Sci., **8** (1978) 21.

[26] R. Blank, J. Magn. Magn. Mater., **83** (1990) 192.